Structure-function analysis of plant aquaporin AtPIP2;1 gating by divalent cations and protons

Lionel Verdoucq, Alexandre Grondin, Christophe Maurel

Title:

Structure-function analysis of plant aquaporin *At*PIP2;1 gating by divalent cations and protons

Authors:

Lionel Verdoucq[#], Alexandre Grondin and Christophe Maurel.

Biochimie et Physiologie Moléculaire des Plantes, Institut de Biologie Intégrative des Plantes, UMR 5004 CNRS, UMR 0386 INRA/ Montpellier SupAgro/ Université Montpellier 2, F-34060 Montpellier Cedex 1, FRANCE

Address correspondence to: Lionel Verdoucq, Biochimie et Physiologie Moléculaire des Plantes, UMR5004, CNRS/INRA/SupAgro/UM2, 2 place Viala, F-34060 Montpellier cedex, France.

[#] Corresponding author: Email: verdoucq@supagro.inra.fr
Tel : +33 499 612 021
Fax : +33 467 525 737

Short title : Divalent cation and pH regulation of plant aquaporin

1

SYNOPSIS

Water channel proteins (aquaporins) of the Plasma membrane Intrinsic Protein (PIP) subfamily provide means for fine and quick adjustments of the plant water status. A molecular model for gating of PIPs by cytosolic protons (H^{+}) and divalent cations was derived from the atomic structure of spinach *So*PIP2;1 in an open- and a closed-pore conformation. Here, we produced in *Pichia pastoris* the *Arabidopsis At*PIP2;1 homolog, either wild-type (WT) or with mutations at residues supposedly involved in gating. Stopped-flow spectrophotometric measurements showed that, upon reconstitution in proteoliposomes, all forms function as water channels. First functional evidence for a direct gating of PIPs by divalent cations was obtained. In particular, cadmium and manganese were identified, in addition to calcium (Ca^{2+}) and H^{+} as potent inhibitors of WT *At*PIP2;1. Our data further show that His[199], the previously identified site for H^{+} sensing, but also N-terminal located Glu[31], and to a lesser extent Asp[28], are involved in both divalent cations and H^{+}-mediated gating. By contrast mutation of Arg[124] rendered *At*PIP2;1 largely insensitive to Ca^{2+} while remaining fully sensitive to H^{+}. The role of these residues in binding divalent cations and/or stabilizing the open or closed pore conformations is discussed.

THIS IS NOT THE FINAL VERSION - see doi:10.1042/BJ20080275

2

Abbreviations footnote:
AQP : aquaporin
Ea : activation energy
k_{exp} : exponential rate constant
PIP : Plasma membrane Intrinsic Protein
P_f : osmotic water permeability
OTG : octyl-β-thioglucopyronoside

THIS IS NOT THE FINAL VERSION - see doi:10.1042/BJ20080275

INTRODUCTION

Water is crucial for life and in most organisms its diffusion across membranes is facilitated by aquaporins (AQP), a conserved family of channel proteins [1]. AQPs assemble as tetramers, each of the monomers defining an individual pore. These monomers exhibit six membrane-spanning α-helices tilted along the plane of the membrane and connected by five loops (*A*-*E*) [2]. In all AQPs, loops *B* and *D*, as well as the N- and C-terminal tails, are bathing in the cytoplasm. To achieve constant adjustment of membrane water permeability in a fast, fluctuating environment, cells have developed multiple controls of AQP function. The regulation of AQP gating, *i.e.* the opening and closing of the pore, allows a rapid and reversible modulation of water transport. In plants, several cellular effectors can affect the intrinsic water permeability of plasma membrane AQPs of the Plasma membrane Intrinsic Protein (PIP) subfamily which, therefore have emerged as a model for studying AQP gating. The water permeability of *Arabidopsis* plasma membrane vesicles was shown to be reversibly inhibited by protons (H^+), with a half inhibition at pH 7.2 [3]. A further structure-function analysis identified a His residue conserved in cytoplasmic loop *D* of all PIPs as central for pH-dependent gating [4]. This study and the determination of the atomic structure of spinach *So*PIP2;1 in an open and a close state [5] also indicated a possible role for residues of loop *D* adjacent to the His [4] or for residues located in the N-terminal tail [5]. In particular, structural models of *So*PIP2;1 suggested that at acidic pH, the channel is maintained in a closed-state by an ionic interaction between the protonated His^{193} residue of loop *D* and the carboxylic sidechain of Asp^{28}, located in the N-terminus of the protein. During pH-induced closure, displacement of loop *D* by 16Å moves the sidechain of Leu^{197} into the lumen of the pore, thereby creating an hydrophobic barrier, and a pore constriction that prevents water permeation.

The activity of water channels in the *Arabidopsis* plasma membrane can also be inhibited by calcium (Ca^{2+}), with an IC50 of 75 μM [3]. A recent study on plasma membranes from *Beta vulgaris* storage roots confirmed these observations [6] and identified both a high (IC50 of 5 nM) and low (IC50 of 200 μM) apparent affinity component for inhibition of membrane water permeability by Ca^{2+}. Recent crystallization of *So*PIP2;1 in the presence of 0.1 M $CdCl_2$ and determination of a structure of the protein in a closed state provided further insights into the gating mechanisms induced by divalent cations, such as Cd^{2+} and presumably Ca^{2+} [5]. In this structure, Asp^{28} and Glu^{31} sidechains directly interact with Cd^{2+}. Upon binding, Cd^{2+} mediates a conformational change of loop *D* and closure of the pore by a network of hydrogen bonding, involving the cytoplasmic sidechain of Arg^{118} in loop *B* and backbone carbonyl groups of Arg^{190} and Asp^{191} in loop *D*. Although Ca^{2+} or other divalent cations may substitute for Cd^{2+} in this model, the defined effects of divalent cations in terms of apparent inhibition constants have remained undefined. As a consequence, the prevalent role proposed for Ca^{2+} in inhibiting water channels *in vivo* has remained uncertain.

In the present work, we performed a structure-function analysis of PIP gating using water transport assays on a purified protein. *At*PIP2;1 represents one of the most highly expressed PIPs in the roots and leaves of *Arabidopsis*. Wild-type (WT), and site-directed mutants of *At*PIP2;1 were produced in the yeast *Pichia pastoris*, purified and reconstituted into proteoliposomes. The effects of a set of divalent cations on the water transport activity of the various *At*PIP2;1 forms provided insights into the molecular basis of cation-dependent gating. Moreover, we showed that pH- and cation-dependent gating can be mechanistically dissociated in some specific mutants.

EXPERIMENTAL

Cloning of WT and site-directed mutants of *At*PIP2;1 for *P. pastoris* expression

The *At*PIP2;1 cDNA was amplified by PCR using 2.5 units (U) of the high fidelity Isis DNA polymerase (MP BioMedicals) and the forward *Eco*RI-*At*PIP2;1 and reverse *At*PIP2;1-*Xho*I primers (table 1) containing the ATG and STOP codons, respectively. Site-directed mutants of *At*PIP2;1, where Asp^{28}, Glu^{31}, Arg^{124} or His^{199} were substituted by an Ala residue, were obtained by PCR-mediated primer extension [7] using the forward *Eco*RI-*At*PIP2;1 and reverse *At*PIP2;1-*Xho*I primers, and a pair of complementary mutated oligonucleotides as listed in table 1. PCR products were cloned into the *P. pastoris* vector pPICZB (Invitrogen) at *Eco*RI and *Xho*I restriction sites. After cloning, the sequence of WT or mutated *At*PIP2;1 was systematically verified by sequencing (Genoscreen, Lille, France). *P. pastoris* was transformed by homologous recombination at the chromosomal *AOX1* locus. For this, the pPICZB vectors containing WT or mutated *At*PIP2;1 cDNAs were linearized with *Sac*I and transferred into the strain X-33 (Invitrogen) using the electroporation method. Transformants were selected on 100 µg/ml zeocin YPDS plates (Invitrogen) according to the manufacter's instructions or on 500 µg/ml zeocin YPDS plates for isolation of "jackpot" clones.

Production of *At*PIP2;1 in *P. pastoris*

Yeast transformants were selected based on an initial small-scale protein production assay [8]. Briefly, after an initial overnight preculture in a glycerol-containing BMGY medium (Invitrogen), cells were inoculated at 22°C (OD_{600} = 1.0) in a methanol-containing BMMY medium (Invitrogen) in baffled flasks with shaking at 225 rpm, to induce recombinant protein expression. Cells were harvested after 24 h and total membrane proteins were extracted as previously described [9]. Immunodetection of *At*PIP2;1 in the extracts [10] was used to select transformants with the highest protein expression level. For large scale production, membranes were extracted using a procedure adapted from [3] and [8]. All steps were realized at 4°C with all buffers supplemented by 1 % of a cocktail of yeast protease inhibitors (Sigma). Cells were resuspended in 5 ml/g cells of an extraction buffer (500 mM saccharose, 10 % glycerol, 20 mM EDTA, 20 mM EGTA, 50 mM NaF, 5 mM β-glycerophosphate, 1 mM phenantroline, 0.6 % PVP, 10 mM ascorbic acid, 5 mM DTT, 1 mM sodium orthovanadate, 50 mM Tris, pH 8) and homogenized by high pressure cavitation at 1200 bars in a Cell Disruptor (Constant System Ltd, Warwick, UK). The lysate was centrifuged for 10 min at 10000 *g* and the resulting surpernatant was further centrifuged for 35 min at 57000 *g*. The final microsomal pellet was resuspended in 330 mM saccharose, 2 mM DTT, 10 mM NaF, 5 mM potassium phosphate buffer, pH 7.8. Membranes were stripped by an urea/alkali treatment [8], resuspended in 10 % glycerol, 2 mM DTT, 10 mM NaF, 20 mM piperazine, pH 9.5, at a protein concentration of about 20 mg/ml and stored at -80°C until use.

Solubilization and purification of *At*PIP2;1

Stripped membranes were diluted to a protein concentration of 2 mg/ml and solubilized in 3 % octyl-β-thioglucopyronoside (OTG; Anatrace, Maumee OH, USA). After 1 h at 28°C, unsolubilized material was pelleted at 100000 *g* for 30 min. *At*PIP2;1 was purified by anion exchange chromatography using 1 ml HiTrap Sepharose HP columns (Amersham). After a first equilibration step in buffer A (0.5 % OTG, 10 % glycerol, 2 mM DTT, 20 mM piperazine, pH 9.5), solubilized proteins were injected into the column and unbound proteins were washed out by 5 ml of buffer A. The retained proteins were then eluted by a linear gradient from 0.1 to 0.65

5

M NaCl in 20 ml of buffer A. Fractions that were the most enriched in *At*PIP2;1 were pooled and *At*PIP2;1 was further concentrated by ultrafiltration on 50 kDa filters (Microcon, Millipore). Proteins concentration was determined by a BCA titration assay (Pierce).

Liposome and proteoliposome reconstitution

Purified *At*PIP2;1 was reconstituted into vesicles of *Escherichia coli* polar lipid extract (Avanti Polar Lipids, Alabaster AL, USA). The lipids were dissolved in a reconstitution buffer (30 mM KCl, 20 mM Tris–Mes, pH 8.3) to a concentration of 2.5 mg/ml and OTG was added at a concentration of 1 % (w/v) to the preformed liposomes. Proteins were added to the liposome solution, at a lipid to protein ratio (LPR) between 16 and 66. After incubation at 28°C for 30 min, proteoliposomes were formed at room temperature by a detergent removal procedure using SM2 polystyrene beads (Biorad). The mass of beads was 30-times the mass of OTG present in the lipid solution [11]. Vesicle size was normalized at 40°C to a mean diameter of 0.2 μm by serial extrusion of the proteoliposomes suspension through a polycarbonate filter (Mini-extruder, Avanti Polar Lipids). Control liposomes were prepared in the same way as the proteoliposomes, except that a pure reconstitution buffer instead of a protein sample was added. Probably due to variable experimental conditions (room temperature during liposome formation, quality/age of the Biobeads used for detergent removal, quality/age of detergent and lipids, …) we were not able to obtain the same specific activity for every reconstitution, even when working at the same LPR and with the same protein extract (Supplemental Table 1). This variability yielded an apparent discrepancy in calculated osmotic water permeability (P_f) values. We checked on a set of 6 independent reconstitutions of *At*PIP2;1, all at LPR 33, with P_f measurements done at pH = 8.3 and 6.0, that the calculated percentage of *At*PIP2;1 P_f inhibition is not dependent on P_f, that is on the reconstitution efficiency of the protein into proteoliposomes. Therefore, we decided to express in the manuscript the results as percentage of initial P_f.

Because divalent cations are not diffusible through lipid bilayers, a modified procedure was required to study their effects on vesicle water transport. In brief, the newly reconstituted vesicles were loaded with 0.6 M glycerol for 2 h and diluted 20-fold in a reconstitution buffer complemented with the indicated concentration of divalent cations. The hypo-osmotic shock associated with vesicle dilution induces a transient opening of vesicles and equilibration of their interior with the extravesicular solution [12]. Resealed vesicles were then extruded at 0.2 μm as described above.

Stopped flow spectrophotometry

Kinetics of vesicle volume adjustment were followed by 90° light scattering at λ_{ex} = 515 nm. Measurements were performed at 15°C, in a SFM3 stopped-flow spectrophotometer (Biologic, Claix, France) essentially as previously described [13]. Briefly, membranes were diluted 10-fold into the reconstitution buffer (105 mosmol.kg^{-1} H$_2$O). Alternatively, membranes were diluted in the same medium but adjusted at a modified pH and incubated for 2 h at room temperature. Vesicles were then loaded in the stopped-flow device and mixed (dead time <3 ms) with an equal volume of the reconstitution buffer but with a concentration of 270 mM mannitol (392 mosmol.kg^{-1} H$_2$O). This resulted in a 144 mosmol.kg^{-1} H$_2$O inward osmotic gradient. The traces from ≥10 individual stopped flow acquisitions were averaged and the curves were fitted to single exponential equations to determine an exponential rate constant k_{exp}. The osmotic water permeability coefficient (P_f) was computed from the light scattering time course and the size of membrane vesicles according to the following equation:

$$P_f = k_{exp}.V_o/A_v.V_w. C_{out}$$

6

where V_o is the initial mean vesicle volume, A_v is the mean vesicle surface, V_w is the molar volume of water, and C_{out} is the external osmolality [13]. Because they were extruded, all vesicle preparations were considered to have a mean diameter of 0.2 µm.

Statistics

Statistical analyses were performed using a Statistica 7 software (StatSoft). Data were analysed using parametric (ANOVA followed by Newman-Keuls tests) and, in case of small samples ($n \leq 6$), non parametric (Mann and Whitney) statistical tests. Results are means ± S.E.M. Differences were considered significant at $p < 0.05$.

RESULTS

Production of *At*PIP2;1 in *P. pastoris*

In order to get hundreds of micrograms of purified *At*PIP2;1, production in *P. pastoris* had first to be optimised. We first observed that when *P. pastoris* transformed strains were grown in the presence of methanol, maximum *At*PIP2;1 levels as monitored by western blots on total protein extracts were reached after 24 h of growth while biomass still increased for an extra day (results not shown). In addition, standard selection of *P. pastoris* strains on 100 µg/ml zeocin led to 60-70 % clones being positive for protein expression. Yet, we selected "jackpot" strains at 500 µg/ml zeocin which, although much more rare, showed a much higher level of *At*PIP2;1 expression than clones selected in standard conditions (results not shown).

Because of our interest in the mechanisms of *At*PIP2;1 gating, we produced a native, untagged form of the protein. Treatment of stripped membranes with OTG was able to fully solubilize *At*PIP2;1 and yielded a protein extract with very few apparent contaminant proteins, as shown by Coomassie blue staining (results not shown). The solubilized protein sample was then fractionated by anionic exchange, and fractions eluted with 0.36-0.42 M NaCl contained most of the *At*PIP2;1 protein which was further concentrated (Figure 1). Mass spectrometry analysis of a tryptic digest of the 28 kDa band shown in Figure 1 revealed that the 8 most abundant peptides corresponded to *At*PIP2;1 (results not shown). An overall yield of ~65 µg *At*PIP2;1 per liter of culture was obtained using this optimized expression procedure.

Functional reconstitution of *At*PIP2;1 in proteoliposomes

*At*PIP2;1 was reconstituted in proteoliposomes at LPRs of 16, 33 and 66 and the water transport properties of the proteoliposomes were compared to those of control *E. coli* liposomes by stopped-flow spectrophotometry. Figure 2 shows light-scattering recordings of the kinetics of liposome volume adjustment in response to a hypertonic challenge imposed at t =0 in a buffer at pH 8.3. The rate constant (k_{exp}) of the exponential curve fitted to the experimental light scattering recordings was 89.1 ± 2.6 s^{-1}, 60.6 ± 4.0 s^{-1} and 21.3 ± 0.9 s^{-1} for proteoliposomes with LPRs of 16, 33 and 66, respectively (Figure 2). Corresponding osmotic water permeability (P_f) values of 691.6 ± 20.2 µm.s^{-1}, 470.2 ± 31.0 µm.s^{-1} and 165.0 ± 7.0 µm.s^{-1} were calculated for the three types of proteoliposomes. Control liposomes were reconstituted, either with the reconstitution buffer alone or with proteins tentatively purified, in the same conditions as *At*PIP2;1, but from untransformed control yeasts. The two control preparations displayed similar k_{exp} values of 3.9 ± 0.1 s^{-1} and 4.3 ± 0.2 s^{-1}, respectively (Figure 2). These correspond to P_f values of 30.6 ± 0.5 µm.s^{-1} and 33.7 ± 1.3 µm.s^{-1}, respectively.

Temperature dependence of water transport indicated activation energy (*Ea*) values of 17.4 kcal.mol^{-1} and 4.0 kcal.mol^{-1} for control liposomes and for *At*PIP2;1 proteoliposomes

7

reconstituted at LPR = 33, respectively (Supplemental Figure 1) The low P_f and high Ea of control liposomes are typical of a lipid-mediated water transport. By contrast, the increased P_f associated to a lower Ea of proteoliposomes containing AtPIP2;1 establish the water channel activity of the reconstituted aquaporin.

pH regulation of AtPIP2;1 water transport activity

To evaluate the H^+-dependency of AtPIP2;1 mediated water transport, proteoliposomes reconstituted at pH 8.3 were diluted 10-fold with an iso-osmotic buffer at pH 6.0, and vesicles were osmotically challenged using an hyper-osmotic buffer also equilibrated at pH 6.0. While a short incubation time (~1 min) in the iso-osmotic buffer at pH 6.0 led to a 50 % decrease in P_f, longer incubations (up to 2 h) gradually decreased P_f to 8 % of its initial value (Supplemental Figure 2). These results suggest that AtPIP2;1 was inserted in the proteoliposomes with about one half of the proteins in an inside-out (cytoplasmic loop D outside) configuration which therefore could be instantaneously blocked by an extravesicular acidification. The time-dependent inhibition of P_f was interpreted as reflecting the time required for H^+ diffusion through the lipid bilayer and blockade of AtPIP2;1 proteins in an outside-out configuration. pH-dependency of AtPIP2;1 activity was then tested after a 2 h incubation at 25°C to allow H^+ equilibration on both sides of the membrane. Figure 3 shows the effect of pH ranging from 3.8 to 9.5 on water transport of vesicles, either control or containing AtPIP2;1. P_f of AtPIP2;1 proteoliposomes was maximal at pH >8 and was decreased by 99 % at pH 3.8, with a half inhibition at pH = 7.15 (± 0.15; n = 2). Hill coefficients deduced from fitted experimental curves were close to unity (h = 1.22 ± 0.23), suggesting a lack of cooperativity between individual monomers during pH-induced channel closure. The pH-dependency of the reconstituted AtPIP2;1 is consistent with measurements realized on plant plasma membrane vesicles or on $Xenopus$ oocytes expressing AtPIP2;2 [3, 4, 6].

Regulation of AtPIP2;1 water transport activity by divalent cations

To evaluate the ability of divalent cations, and Ca^{2+} in particular, to directly gate AtPIP2;1, 1 mM $CaCl_2$ was added directly on proteoliposomes in an iso-osmotic solution 3 min prior to the water transport assay. This treatment resulted in a ~50 % inhibition of P_f (data not shown). To ensure that Ca^{2+} had access to the interior of the vesicles and could block AtPIP2;1 in either orientation, proteoliposomes were submitted to a sudden hypo-osmotic shock in the presence of 1 mM $CaCl_2$. This shock induces a transient opening of the vesicles and equilibration of their interior with the extra-vesicular solution [12]. Under these conditions, the P_f of AtPIP2;1 vesicles was reduced by 86 % (results not shown). We also checked that a similar hypotonic treatment in the presence of Ca^{2+} did not alter the P_f of control liposomes (results not shown). In experiments where the concentration of free Ca^{2+} was varied between 0 and 5 mM (Figure 4), we observed a monophasic dose-response curve with an apparent IC50 of 42 ± 25 µM (n = 5). The fitted Hill coefficient was close to unity (h = 0.83 ± 0.11) suggesting a lack of cooperativity during the process of Ca^{2+}-dependent P_f inhibition. These data provide evidence that Ca^{2+} can act directly on AtPIP2;1 to induce pore closure.

Effects of a series of divalents cations on P_f of AtPIP2;1 vesicles were compared at a fixed concentration of 150 µM (Figure 5). We tested divalent cations that either belong to the same alkaline earth metal series as Ca^{2+} (Mg^{2+}, Ba^{2+}, Sr^{2+}), display a similar atomic radius (Mn^{2+}), or are known to bind to plant SoPIP2;1 (Cd^{2+}) or to regulate activity of animal AQPs (Ni^{2+}) [5, 14]. In addition, we tested the effects of mercury ions (Hg^{2+}) which have been reported as common AQP blockers [15]. Surprisingly, Hg^{2+} was not able to inhibit the P_f of AtPIP2;1 vesicles (Figure

8

5). Mg^{2+} did not alter significantly water transport in AtPIP2;1 vesicles either whereas Ca^{2+} inhibited P_f by 60 %. Sr^{2+}, Ba^{2+} and Ni^{2+} reduced the P_f by 40 %, 37 % and 48 %, respectively. Mn^{2+} induced an inhibition of P_f by 60 %, similar to Ca^{2+}. Cd^{2+} was the most effective cation with an inhibition of P_f by 70 % (Figure 5). Dose-response experiments for inhibition of P_f in AtPIP2;1 vesicles by Cd^{2+}, Mn^{2+} and Ni^{2+} indicated apparent IC50 values of 27 ± 13 µM, 85 ± 37 µM and 178 ± 46 µM, respectively (Figure 6). This set of data clearly indicates that AtPIP2;1 can be blocked by a wide range of divalent cations with distinct sensitivities, Ca^{2+} being one of the most efficient blockers.

Cytoplasmic determinants for regulation of AtPIP2;1 by divalent cations and pH

To examine the molecular bases of AtPIP2;1 sensitivity to H^+ or divalent cations, we investigated the effects of point mutations of four residues that may be involved in these regulations. We selected Asp^{28}, Glu^{31}, Arg^{124} and His^{199}, based on the possible role of the corresponding residues of SoPIP2;1, as was proposed from the atomic structures of the protein in an open and closed states [5]. The four residues were individually mutated to Ala residues and the resulting D28A, E31A, R124A and H199A forms were expressed in $P.$ $pastoris$ and purified as described for wild-type AtPIP2;1 (WT) (Supplemental Figure 4). In this series of experiments, functional reconstitution of the mutant or WT proteins sometimes failed at the highest protein content (LPR range: 16-33). Therefore, we analysed P_f of proteoliposomes reconstituted at a lower protein content (LPR range: 33-40), which however ensured a very significant contribution of AQPs to P_f (Supplemental Figure 3). When compared at similar LPR, the increased water channel activity of proteoliposomes containing the WT or mutant proteins indicated that no major change in intrinsic water permeability had been induced by either one of the introduced mutations (results not shown). The sensitivities of mutant and WT proteins to H^+ were compared at pH = 6.0 (Figure 7A) and at intermediate blocking conditions by divalent cations (Ca^{2+}, Cd^{2+} and Mn^{2+}, all at 150 µM), to discriminate more easily between weakly and strongly affected mutants (Figure 7B).

The R124A mutant showed an inhibition of P_f by H^+ (84.4 ± 1.5 %), not significantly different to that of WT (83.7 ± 2.8 %) (Figure 7A). By contrast, the H199A mutant was almost insensitive to H^+ (5.5 ± 4.0 %) while the D28A and E31A forms showed intermediate P_f inhibitory responses by 54.3 ± 4.4 % and 56.5 ± 4.6 %, respectively. These results confirm a central role for His^{199} in H^+-induced pore closure and provide the first functional data for a role of the N-terminal tail in this process.

In parallel experiments, the WT form showed a P_f inhibition of 39.8 ± 8.1 %, 61.0 ± 5.8 % and 50.0 ± 7.7 % in response to 150 µM of Ca^{2+}, Cd^{2+}, and Mn^{2+}, respectively. With respect to the WT form, the D28A mutant showed a tendency to lower inhibition by the three divalent cations (27.1 ± 8.8 %, 43.8 ± 9.8 % and 41.3 ± 6.8 %). By contrast, the E31A mutation had significant effects on Ca^{2+} and Cd^{2+} sensitivities, with a P_f inhibition of 6.4 ± 7.1 % and 21.6 ± 14.2 %, respectively. Yet, the inhibition of P_f by Mn^{2+} (36.8 ± 7.9 %) was similar to that of the WT form. The R124A form was significantly affected in its P_f sensitivity to all divalent cations and the percentages of inhibition by Ca^{2+} (10.0 ± 5.7 %), Cd^{2+} (18.7 ± 11.2 %) and Mn^{2+} (26.3 ± 7.0 %) were all reduced by >2-fold with respect to those of the WT form. Finally, the H199A mutant also showed a very poor sensitivity to divalent cations with a P_f inhibition of 3.9 ± 7.9 %, 11.6 ± 13.7 % and 4.9 ± 14.0 % in response to 150 µM of Ca^{2+}, Cd^{2+} and Mn^{2+}, respectively. Dose-dependent effects of Ca^{2+}, Cd^{2+} and Mn^{2+} on P_f of liposomes (control) and proteoliposomes reconstituted with AtPIP2;1, either WT or mutant (D28A, E31A, R124A and H199A) forms are shown in Supplemental Figure 4. These experiments showed a relative insensitivity of the four

9

mutants to high Ca^{2+} concentration (1 mM). By contrast, a similar concentration of Cd^{2+} and Mn^{2+} was able to fully inhibit the R124A mutant form while being poorly active on D28A, E31A, and H199A. In conclusion, these analyses showed that all tested residues (Asp^{28}, Glu^{31}, Arg^{124}, and His^{199}) are, although to different extent, involved in divalent cation-dependent gating of AtPIP2;1. Furthermore, substitution of Glu^{31} by an Ala residue reveals a striking ability of the mutant protein to discriminate between distinct divalent cations.

DISCUSSION

The present work reports on the reconstitution in proteoliposomes of AtPIP2;1, one of the most highly expressed PIPs in *Arabidopsis*. The protein conferred on liposomes extremely high water permeability with P_f levels exceeding 1000 $\mu m.s^{-1}$. Noticeably, these values are similar to those obtained with animal AQPs [16] and are the highest obtained for a reconstituted plant aquaporin [8, 17]. PIP aquaporins have been described to be post-translationally regulated by several factors or modifications, such as H^+, free Ca^{2+} or Ser phosphorylation, all acting on the cytosolic side of the protein [3, 4, 6, 18]. While functional expression of PIPs in *Xenopus* oocytes was instrumental for deciphering the regulation of water channel activity by H^+ and phosphorylation, structure-function studies addressing the regulation of PIPs by divalent cations have been lacking.

Here, we demonstrated that the water channel activity of AtPIP2;1 can be fully blocked by H^+, with a half-inhibition at pH 7.15. In addition, AtPIP2;1 was shown to be inhibited by divalent cations, with the highest efficiency for Ca^{2+}, Cd^{2+}, and Mn^{2+}. With respect to previous studies on plasma membrane vesicles purified from plants, the present work represents the first description of the direct inhibition of an individual PIP isoform by divalent cations. In particular, AtPIP2;1 showed an IC50 of 42 μM ($\pm$ 25 μM) for Ca^{2+}-mediated P_f inhibition which is in good agreement with the IC50 of 75 μM observed for plasma membrane vesicles from *Arabidopsis* suspension cells [3]. By contrast, Ca^{2+}-dependent inhibition of P_f in plasma membranes from *Beta vulgaris* storage roots [6] showed both a high (IC50 ~ 5 nM) and a low (IC50 ~ 200 μM) apparent affinity component. Because of their conserved structure, all PIP isoforms are likely to be blocked by Ca^{2+} but may differ in their sensitivity. The response of *Beta vulgaris* plasma membrane, which composition in AQPs is unknown, may reflect this heterogeneity. Because PIPs can be divided in two subclasses, PIP1 and PIP2, it will be interesting to determine the sensitivity of PIP1s to Ca^{2+} inhibition. Surprisingly, AtPIP2;1 was not inhibited by mercury ions although it has the same conserved Cys residues as most other PIPs. Nevertheless, our observations are consistent with previous studies in *Xenopus* oocytes showing that AtPIP2;1 was insensitive to 1 mM $HgCl_2$ whereas four other *Arabidopsis* PIP isoforms (AtPIP1;1, AtPIP1;2, AtPIP1;3 and AtPIP2;2) were significantly blocked [19].

Because the *in vitro* inhibition of PIPs by divalent cations such as Ca^{2+} or Cd^{2+} exhibits a relatively low sensitivity, the physiological significance of this phenomenon has been questioned. Peak free Ca^{2+} concentrations of a few μM have been measured in the plant cytosol [20]. However, free Ca^{2+} may locally reach higher concentrations, especially in the close vicinity of Ca^{2+} channels. In these respects, PIPs were found in detergent resistant membranes [21, 22] where they may cluster with other membrane transport proteins. Exposure of plants to trace concentrations of Cd^{2+} leads to accumulation of this highly toxic ion in plant cells and can affect the plant-water relations [23, 24]. Our results suggest that one basis of these effects may be a direct gating of PIPs by the ion.

10

The atomic structure of spinach *So*PIP2;1 in an open and a closed conformation [5] has provided a landmark advance for investigating the molecular determinants of PIP gating. The present structure-function approach provides a step forward and allows to confirm and refine the proposed model [5]. The atomic structure of *So*PIP2;1 in the closed state showed a Cd^{2+} ion in a close vicinity of the Asp^{28} and Glu^{31} residues [5]. Although the D28A mutant shows a tendency to a lower inhibition by divalent cations, our data establish a clear functional role for Glu^{31} only. The data suggest that the latter residue is the main actor of this process, probably due to a higher flexibility of the Glu than the Asp sidechain [25]. The role of Glu^{31} in primarily binding the ion is further supported by the finding that its mutation selectively altered Ca^{2+}, and to a lesser extent Cd^{2+} inhibition of P_f, whereas it did not altered significantly Mn^{2+} inhibition. This is in agreement with the notion that Ca^{2+} usually displays higher coordination numbers than Cd^{2+} or Mn^{2+} [26]. Similar to Glu^{31}, substitution of Arg^{124} drastically altered gating of PIPs in response to Ca^{2+} and Cd^{2+}. Here, our results support the proposed role of this residue in bridging the N-terminal binding site of ions with loop *D*, in order to stabilize the closed conformation of the pore (Figure 8). We note however that, since Glu^{31} and Arg^{124} likely form hydrogen bonds [5], each of the two residues may actually contribute to both ion binding and stabilization of the closed-pore conformation. More unexpectedly, our analysis uncovered a role for His^{199} in loop *D* in divalent cation dependent-gating. Here, the analysis of the open and the closed conformations is not giving a direct clue to explain this result. We propose that the mutation of this or neighbouring residues may alter loop *D* local structure and unstabilize the closed conformation, leading to a constitutively open pore.

The present work also provides insights into the mechanism of PIP gating by H^+. Firstly, we confirmed, by an independent approach, that a conserved His in the loop *D* of all PIPs is a major H^+ sensor [4]. In view of the results discussed above, we cannot, however, rule out the hypothesis that substitution of His199 alters loop *D* local conformation, thus leading to an apparent H^+-insensitivity. However, the half inhibition of P_f at pH = 7.15 supports the hypothesis that residue with a near neutral pKa, that is a His residue, acts as sensor. From the atomic structure of *So*PIP2;1 in a closed conformation, it was proposed that the protonated His would interact through a salt bridge with the carboxylic group of residue 28, found as a Glu or an Asp, in PIP1s and in PIP2s, respectively [5]. Our structure-function analysis confirms this interaction but also unravels a role for Glu^{31}. Therefore, our study indicates a flexibility for the salt bridge which again was not deduced from the atomic structure. Interestingly, conserved charged residues adjacent of the loop *D* His (namely Arg^{196} and Asp^{197} in *At*PIP2;1) can confer, after mutation to Ala, H^+-insensitivity to the protein [4]. A closed-conformation model of *At*PIP2;1 suggest that Asp^{197} could make a salt bridge with the N-terminal Lys^{33}, conserved in most PIP2s (Figure 8). Noticeably, this positively charged residue is not found in PIP1s and these AQPs may possibly exhibit a sensitivity to H^+ slightly different from that of PIP2s.

Changes in H^+ and free Ca^{2+} concentrations in the cytosol are used by plant cells, independently or in combination to transduce developmental, hormonal or stress signals [27-30]. One well identified downstream effect of Ca^{2+} is the stimulation of Ca^{2+}-dependent protein kinases, which have been reported to act on PIPs [18]. Therefore, PIP gating is the converging point of multiple cell signalling mechanisms. The atomic structure of PIPs together with the present structure/function analysis show that the gating of PIPs by H^+ and divalent cations relies at least in part on common molecular mechanisms. The present work also allowed to identify mechanisms that are specific for divalent cation-dependent gating. In particular, we showed that, although Arg^{124} is not directly involved in ion binding, a R124A mutant was largely insensitive to Ca^{2+} while remaining fully sensitive to H^+. The expression in transgenic plants of this type of

11

mutant will be instrumental to test for the physiological significance and specific contribution of divalent cations in AQP gating and regulation of the whole plant water status. Phosphorylation of PIP2s in loop *B* and in the C-terminal tail are also supposed to exert a control of pore opening and closing [18, 31]. Therefore, a next step to add to our approach will be to understand the interplays between the multiple phosphorylated states of PIPs and their direct gating by H^+ and Ca^{2+}.

REFERENCES

1   Agre, P. (1998) Aquaporin null phenotypes: The importance of classical physiology. Proc Natl Acad Sci USA. **95**, 9061-9063

2   Fujiyoshi, Y., Mitsuoka, K., de Groot, B. L., Philippsen, A., Grubmüller, H., Agre, P. and Engel, A. (2002) Structure and function of water channels. Curr. Opin. Struct. Biol. **12**, 509-515

3   Gerbeau, P., Amodeo, G., Henzler, T., Santoni, V., Ripoche, P. and Maurel, C. (2002) The water permeability of *Arabidopsis* plasma membrane is regulated by divalent cations and pH. Plant J. **30**, 71-81

4   Tournaire-Roux, C., Sutka, M., Javot, H., Gout, E., Gerbeau, P., Luu, D. T., Bligny, R. and Maurel, C. (2003) Cytosolic pH regulates root water transport during anoxic stress through gating of aquaporins. Nature. **425**, 393-397

5   Tornroth-Horsefield, S., Wang, Y., Hedfalk, K., Johanson, U., Karlsson, M., Tajkhorshid, E., Neutze, R. and Kjellbom, P. (2006) Structural mechanism of plant aquaporin gating. Nature. **439**, 688-694

6   Alleva, K., Niemietz, C. M., Sutka, M., Maurel, C., Parisi, M., Tyerman, S. D. and Amodeo, G. (2006) Plasma membrane of *Beta vulgaris* storage root shows high water channel activity regulated by cytoplasmic pH and a dual range of calcium concentrations. J Exp Bot. **57**, 609-621

7   Ho, S. N., Hunt, H. D., Horton, R. M., Pullen, J. K. and Pease, L. R. (1989) Site-directed mutagenesis by overlap extension using the polymerase chain reaction. Gene. **77**, 51-59

8   Karlsson, M., Fotiadis, D., Sjovall, S., Johansson, I., Hedfalk, K., Engel, A. and Kjellbom, P. (2003) Reconstitution of water channel function of an aquaporin overexpressed and purified from *Pichia pastoris*. FEBS Lett. **537**, 68-72

9   Daniels, M. J., Wood, M. R. and Yeager, M. (2006) In vivo functional assay of a recombinant aquaporin in Pichia pastoris. Appl Environ Microbiol. **72**, 1507-1514

10   Santoni, V., Verdoucq, L., Sommerer, N., Vinh, J., Pflieger, D. and Maurel, C. (2006) Methylation of aquaporins in plant plasma membrane. Biochem. J. **400**, 189-197

11   Rigaud, J. L. and Levy, D. (2003) Reconstitution of membrane proteins into liposomes. Methods Enzymol. **372**, 65-86

12   Biber, J., Malmström, K., Scalera, V. and Murer, H. (1983) Phosphorylation of rat kidney proximal tubular brush border membranes. Role of cAMP dependent protein phosphorylation in the regulation of phosphate transport. Pflügers Arch. **398**, 221-226

13   Maurel, C., Tacnet, F., Guclu, J., Guern, J. and Ripoche, P. (1997) Purified vesicles of tobacco cell vacuolar and plasma membranes exhibit dramatically different water permeability and water channel activity. Proc. Natl. Acad. Sci. U S A. **94**, 7103-7108

14   Zelenina, M., Bondar, A. A., Zelenin, S. and Aperia, A. (2003) Nickel and extracellular acidification inhibit the water permeability of human aquaporin-3 in lung epithelial cells. J Biol Chem. **278**, 30037-30043

15   Yukutake, Y., Tsuji, S., Hirano, Y., Adachi, T., Takahashi, T., Fujihara, K., Agre, P., Yasui, M. and Suematsu, M. (2008) Mercury chloride decreases the water permeability of aquaporin-4-reconstituted proteoliposomes. Biol Cell. **100**, 355-363

16   Liu, K., Nagase, H., Huang, C. G., Calamita, G. and Agre, P. (2006) Purification and functional characterization of aquaporin-8. Biol Cell. **98**, 153-161

17   Nyblom, M., Oberg, F., Lindkvist-Petersson, K., Hallgren, K., Findlay, H., Wikstrom, J., Karlsson, A., Hansson, O., Booth, P. J., Bill, R. M., Neutze, R. and Hedfalk, K. (2007)

13

Exceptional overproduction of a functional human membrane protein. Protein Expr Purif. **56**, 110-120

18   Johansson, I., Karlsson, M., Shukla, V. K., Chrispeels, M. J., Larsson, C. and Kjellbom, P. (1998) Water transport activity of the plasma membrane aquaporin PM28A is regulated by phosphorylation. Plant Cell. **10**, 451-460

19   Kammerloher, W., Fischer, U., Piechottka, G. P. and Schäffner, A. R. (1994) Water channels in the plant plasma membrane cloned by immunoselection from a mammalian expression system. Plant Journal. **6**, 187-199

20   Lecourieux, D., Ranjeva, R. and Pugin, A. (2006) Calcium in plant defence-signalling pathways. New Phytol. **171**, 249-269

21   Mongrand, S., Morel, J., Laroche, J., Claverol, S., Carde, J. P., Hartmann, M. A., Bonneu, M., Simon-Plas, F., Lessire, R. and Bessoule, J. J. (2004) Lipid rafts in higher plant cells: purification and characterization of Triton X-100-insoluble microdomains from tobacco plasma membrane. J Biol Chem. **279**, 36277-36286

22   Morel, J., Claverol, S., Mongrand, S., Furt, F., Fromentin, J., Bessoule, J. J., Blein, J. P. and Simon-Plas, F. (2006) Proteomics of plant detergent-resistant membranes. Mol Cell Proteomics. **5**, 1396-1411

23   Poschenrieder, C., Gunse, B. and Barcelo, J. (1989) Influence of Cadmium on Water Relations, Stomatal Resistance, and Abscisic Acid Content in Expanding Bean Leaves. Plant Physiol. **90**, 1365-1371

24   Perfus-Barbeoch, L., Leonhardt, N., Vavasseur, A. and Forestier, C. (2002) Heavy metal toxicity: cadmium permeates through calcium channels and disturbs the plant water status. Plant J. **32**, 539-548

25   Cates, M. S., Teodoro, M. L. and Phillips, G. N., Jr. (2002) Molecular mechanisms of calcium and magnesium binding to parvalbumin. Biophys J. **82**, 1133-1146

26   Oberhauser, A., Alvarez, O. and Latorre, R. (1988) Activation by divalent cations of a Ca^{2+}-activated K^+ channel from skeletal muscle membrane. J. Gen. Physiol. **92**, 67-86

27   Yakir, E., Hilman, D., Harir, Y. and Green, R. M. (2007) Regulation of output from the plant circadian clock. Febs J. **274**, 335-345

28   Israelsson, M., Siegel, R. S., Young, J., Hashimoto, M., Iba, K. and Schroeder, J. I. (2006) Guard cell ABA and CO_2 signaling network updates and Ca^{2+} sensor priming hypothesis. Curr Opin Plant Biol. **9**, 654-663

29   Fan, L. M., Zhao, Z. and Assmann, S. M. (2004) Guard cells: a dynamic signaling model. Curr Opin Plant Biol. **7**, 537-546

30   Shimazaki, K., Doi, M., Assmann, S. M. and Kinoshita, T. (2007) Light regulation of stomatal movement. Annu Rev Plant Biol. **58**, 219-247

31   Johansson, I., Larsson, C., Ek, B. and Kjellbom, P. (1996) The major integral proteins of spinach leaf plasma membranes are putative aquaporins and are phosphorylated in response to Ca^{2+} and apoplastic water potential. Plant Cell. **8**, 1181-1191

TABLE 1 Oligonucleotide primer sequences

Name	orientation	Sequence
*Eco*RI-*At*PIP2;1	sens	GC**GAATTC**AAA<u>AT</u>GGCAAAGGATGTGGAAGCC
*At*PIP2;1-*Xho*I	antisens	GA**CTCGAG**<u>TTA</u>GACGTTGCCAGCACTTC
D28A:Ps	sens	GCTCCGTTTATT*GCT*GGAGCGGAG
D28A:Pa	antisens	CTCCGCTCC*AGC*AATAAACGGAGC
E31A:Ps	sens	GATGGAGCG*GCT*CTAAAGAAGTGG
E31A:Pa	antisens	CCACTTCTTTAG*AGC*CGCTCCATC
R124A:Ps	sens	GTGTCGTTACCT*GCG*GCCCTATTGTAC
R124A:Pa	antisens	GTACAATAGGGC*CGC*AGGTAACGACAC
H199A:Ps	sens	GCTAGAGACTCC*GCC*GTTCCGGTGTTGG
H199A:Pa	antisens	CCAACACCGGAAC*GGC*GGAGTCTCTAGC

The primers were used for the mutation and cloning of WT and mutated forms of *At*PIP2;1 in an pPICZ-B vector (Invitrogen), as described in the experimental section. All primers are given in the 5' to 3' orientation. Cloning sites are indicated in bold characters, mutated/inserted residues are indicated in italics and the start/stop codons are underlined.

15

FIGURE LEGENDS

Figure 1 : SDS-PAGE profile of purified *At*PIP2;1. Protein extracts eluted from Hitrap Q HP columns were obtained from *P. pastoris* strains, either control or expressing *At*PIP2;1. Proteins were stained by Coomassie brilliant blue R250. The two arrows represent monomeric and dimeric forms of *At*PIP2;1.

Figure 2: Stopped-flow light scattering recordings of water transport in liposomes and proteoliposomes containing *At*PIP2;1 at different LPRs. All measurements were performed with solutions at pH 8.3. Imposition of a hyperosmotic gradient at t = 0 causes a shrinkage of the vesicles that can be monitored by a time-dependent change in light scattering. Control liposomes reconstituted with the liposome buffer alone (control) or with proteins tentatively purified from control yeasts (empty plasmid) show typically slow light scattering kinetics. Proteoliposomes reconstituted with increasing amounts of *At*PIP2;1 (LPRs of 66, 33 and 16) show a dose-dependent increase in the rate of vesicle volume adjustment. For each type of reconstitution, the traces from ≥10 individual stopped flow acquisitions were averaged and the curves were fitted to single exponential equations to determine an exponential rate constant k_{exp}. Mean values are indicated in the text. The inset shows a close up of the recordings between 0 and 0.4 s.

Figure 3: Effects of pH on P_f of liposomes and proteoliposomes containing *At*PIP2;1. Control liposomes and proteoliposomes were equilibrated for 2 h at the indicated pH and stopped-flow measurements were performed, as exemplified in Figure 2. P_f was calculated from the exponential rate constants (k_{exp}) fitted from the time course of scattered light intensity and from the size of the extruded vesicles (diameter of 0.2 μm). The figure shows representative data obtained on a same protein reconstitution experiment at a LPR of 16, with stopped-flow measurements made in triplicate (*n*=4). Results are mean ± SEM.

Figure 4: Effects of Ca^{2+} on P_f of liposomes (control) and proteoliposomes containing *At*PIP2;1 (*At*PIP2;1). Vesicles were equilibrated for 3 h in 0.65 M glycerol, and subsequently submitted to a sudden hypo-osmotic shock in the presence of the indicated Ca^{2+} concentrations at pH 8.3. This shock induces a transient opening of the vesicles and equilibration of their interior with the extra-vesicular solution. P_f was determined by stopped-flow recordings as exemplified in Figure 2. The figure shows representative data obtained on a same protein reconstitution experiment at a LPR of 33, with stopped-flow measurements made in triplicate (*n*=3). Results are mean ± SEM.

Figure 5: Effects of a series of divalent cations on P_f of liposomes (control) and proteoliposomes reconstituted with *At*PIP2;1 (*At*PIP2;1). Vesicles were equilibrated, as explained in the legend of Figure 4, with 150 μM of the indicated divalent cations, all provided as chloride salts, and at pH 8.3. P_f was measured using the indicated procedure. Ø represents measurements in a buffer in the absence of any divalent cation. The figure shows (except for $HgCl_2$) representative data obtained on a same protein reconstitution experiment, at a LPR of 33. The absolute P_f value of proteoliposomes in control conditions was 380.4 ± 41.5 $\mu m.s^{-1}$. Stopped-flow measurements were made in triplicate (*n*=3). Results as expressed as mean % (± SEM) of P_f of untreated proteoliposomes. In parallel experiments (not shown), we checked that all ions investigated had no significant effect on the P_f of control liposomes.

16

Figure 6: Dose-dependent effects of Cd^{2+}, Mn^{2+} and Ni^{2+} on P_f of proteoliposomes containing *At*PIP2;1. Procedures and conventions are as in Figure 4. The curve fitted from concentration-dependent effects of Ca^{2+} on P_f (see Figure 4) is shown as a dotted line. Results are mean ± SEM.

Figure 7: Effects of H^+ and divalent cations on P_f of proteoliposomes containing *At*PIP2;1, either WT (WT) or with the indicated mutations (D28A, E31A, R124A, H199A). For all *At*PIP2;1 forms a P_f value was measured at pH =8.3, in the absence of divalent cations, and subtracted by the P_f value of control liposomes ($P_f = 28.7 \pm 1.8$ µm.s^{-1}). The derived P_f values, which reflect the full water transport activity of each of the *At*PIP2;1 forms in the reconstituted proteoliposomes were: WT, $P_f = 542.0 \pm 56.1$ µm.s^{-1}; D28A, $P_f = 390.5 \pm 104.1$ µm.s^{-1} ; E31A, $P_f = 329.4 \pm 92.1$ µm.s^{-1} ; R124A: $P_f = 461.7 \pm 71.3$ µm.s^{-1}; H199A $P_f = 270.8 \pm 39.7$ µm.s^{-1}. These P_f values were used as a reference to calculate the relative P_f inhibition observed in the indicated conditions. Proteoliposome equilibration and stopped-flow measurements were performed at pH 6.0 (A) or in the presence of 150 µM of indicated cations (B). Numbers indicate the number of independent proteoliposome reconstitutions, from at least three independent protein productions. For each reconstitution, H^+- or divalent cation-dependent inhibition was characterized in triplicate stopped-flow assays. Results are mean SEM. *: differs from WT at *p* <0.05.
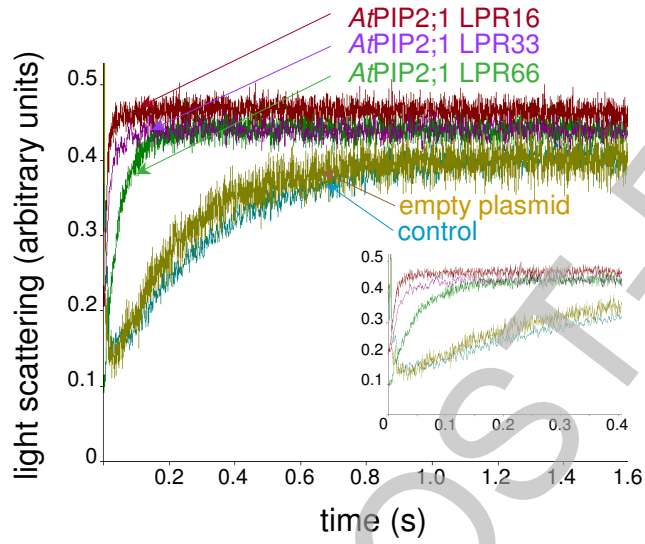
Figure 8: Interpretative model of PIP2 gating by H^+ and divalent cations. Close-up view of the H^+ and divalent cation-binding site of a closed-conformation model of *At*PIP2;1 generated by homology modelling from the *So*PIP2;1 closed-conformation structure (PDB code 1Z98). The location of the divalent cation is shown in purple. Putative salt bridges between His^{199} and Asp^{28}, Glu^{31} and Arg^{124}, and between Asp^{197} and Lys^{33} side chains are represented. Numbers are distances in Å.

17

Figure 1
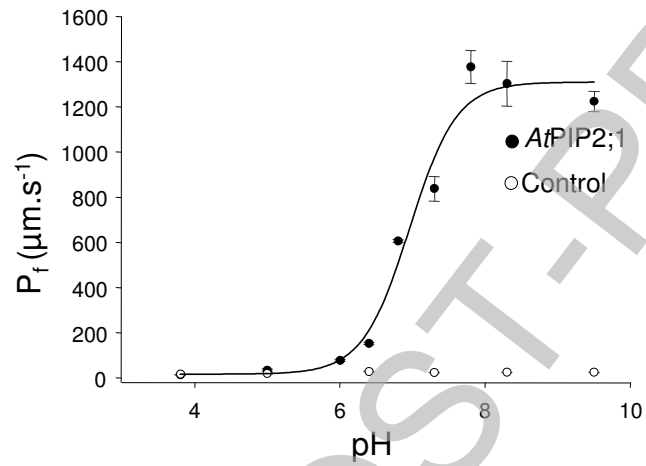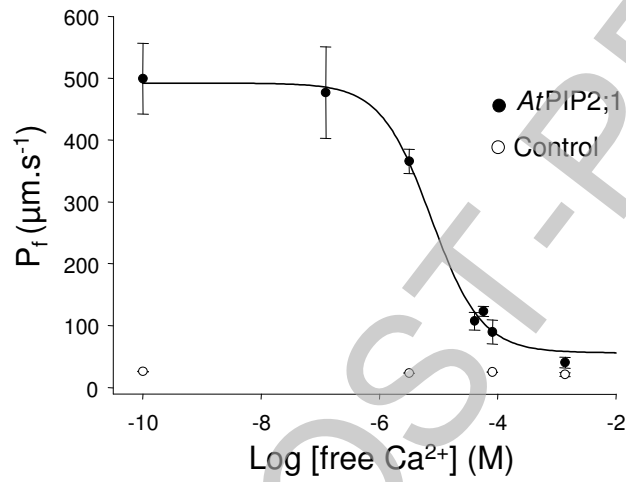
Figure 2

Figure 3
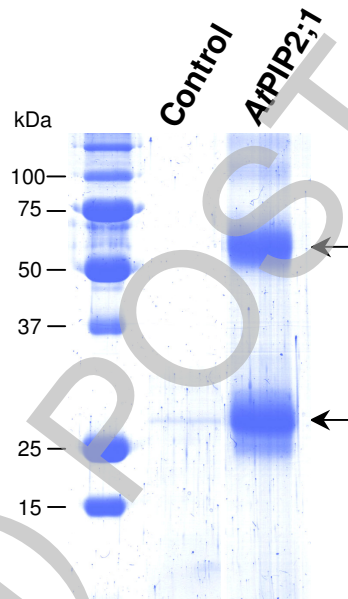
Figure 4

Figure 5

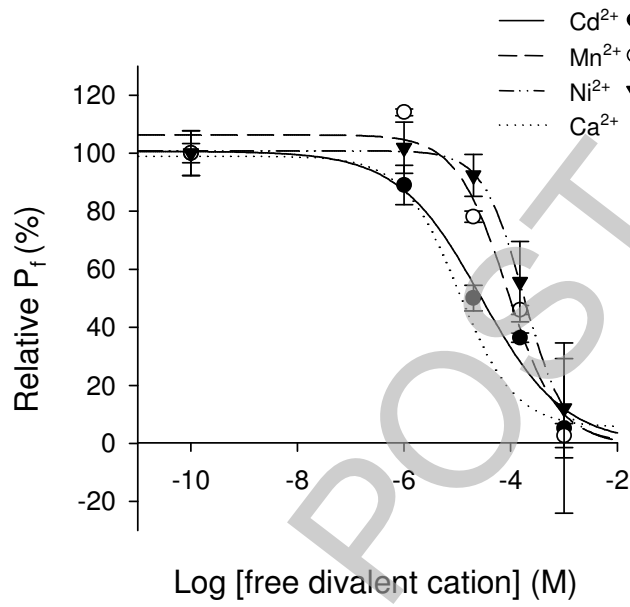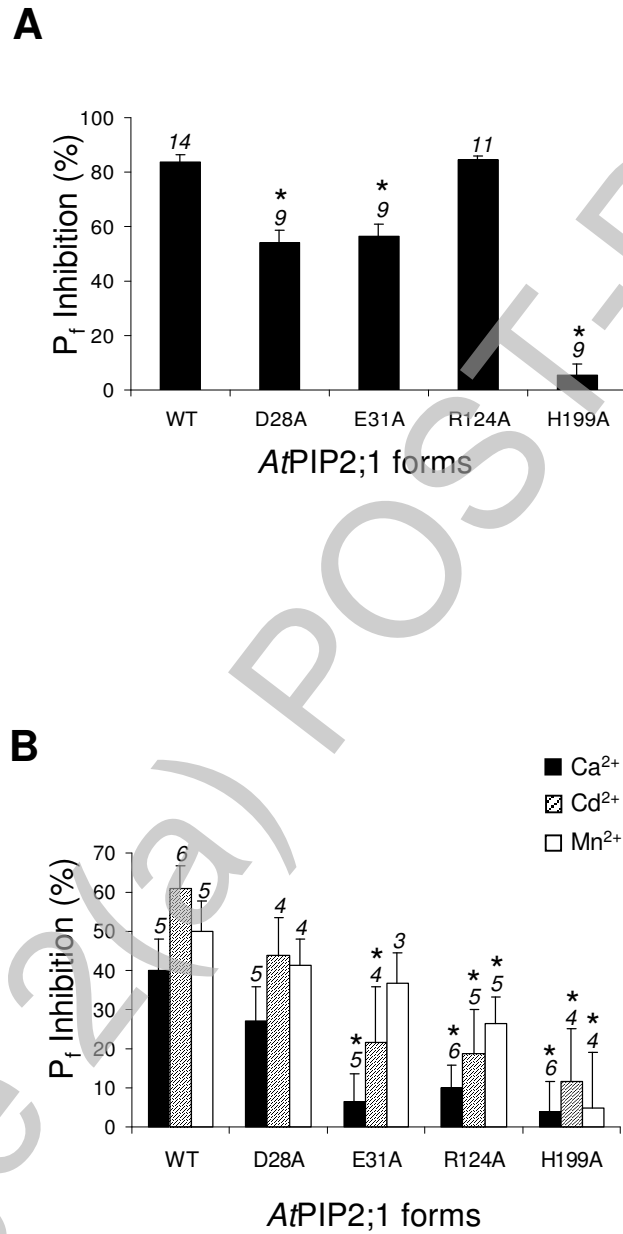THIS IS NOT THE FINAL VERSION - see doi:10.1042/BJ20080275

Figure 6

Figure 7

A

B

Figure 8